Averaging and the Shape of the Correlation Function

Boris Tomášik [1,2,*] , **Jakub Cimerman** [2] **and Christopher Plumberg** [3]

[1] Faculty of Natural Sciences, Univerzita Mateja Bela, Tajovského 40, 97401 Banská Bystrica, Slovakia
[2] FJFI, České vysoké učení technické v Praze, Břehová 7, 11519 Praha 1, Czech Republic; jakub.cimerman@gmail.com
[3] Department of Astronomy and Theoretical Physics, Lund University, Sölvegatan 14A, SE-223 62 Lund, Sweden; astrophysicist87@gmail.com
[*] Correspondence: boris.tomasik@cern.ch

Abstract: A brief pedagogical introduction to correlation femtoscopy is given. We then focus on the shape of the correlation function and discuss the possible reasons for its departure from the Gaussian form and better reproduction with a Lévy stable distribution. With the help of Monte Carlo simulations based on asymmetric extension of the Blast-Wave model with resonances we demonstrate possible influence of averaging over many events and integrating over wide momentum bins on the shape of the correlation function. We also show that the shape is strongly influenced by the use of the one-dimensional parametrisation in the q_{inv} variable.

1. Introduction

Correlation femtoscopy is widely used in heavy-ion collisions for the determination of space–time characteristics of hadron-emitting sources. Most commonly, the two-particle correlation functions are fitted by a Gaussian parametrisation augmented with correction terms due to final-state interactions. The widths of this parametrisation are interpreted in terms of space–time (co-)variances of the homogeneity regions [1–5].

Nevertheless, clear indications exist, that the real shape of the correlation function is not Gaussian, as we could also see in a few talks at the 2018 Zimányi School (see e.g., [6–8]). The shape is often better reproduced by a fit with Lévy stable distribution [9]. The choice of this distribution is not random. Stability is a generalisation of the concept of Central Limit Theorems. Lévy stable distributions possess the property that the shape remains unchanged when one more elementary random process is added to the ones which are already accounted for. The excitement about this particular parametrisation is supported by the argument that with the help of such a fit one could access the critical exponents of the strongly interacting matter [10]. We will show in this paper that the observed shape can be caused by more mundane non-critical phenomena. Mostly, we are interested in the role of averaging in influencing the shape of the correlation function. Note that here we shall only be interested in correlation functions from nuclear collisions.

These ideas set out the outline of this contribution. We first review the basic relations of correlation femtoscopy. Then we particularly look at the Lévy stable parametrisations and scrutinise various effects that can lead to such a shape of the correlation function.

2. The Formalism of Correlation Femtoscopy

The two-particle correlation function is constructed in such a way as to reveal the effect of correlations. Since this is a school, we stay on a pedagogical level and introduce the main elements of

correlation femtoscopy one by one. For pion pairs one usually uses the correlation stemming from the symmetrisation of the wave function. Nevertheless, the effect of final state interactions is always present, as well. They can be due to electromagnetic or strong interactions. For identical charged pions, the electromagnetic Coulomb final state interactions are important. We shall assume here, that their influence can be factored out from the data with the help of a correction factor [11,12].

The correlation function is then experimentally obtained as

$$C(p_1, p_2) = \frac{P(p_1, p_2)}{P_{\mathrm{mix}}(p_1, p_2)},$$ (1)

where $P(p_1, p_2)$ is the two-particle distribution in the momenta, and $P_{\mathrm{mix}}(p_1, p_2)$ is an analogous distribution in which each particle comes from a different event. Due to wave function symmetrisation for boson pairs, the correlation function exhibits a peak for small momentum differences $p_1 - p_2$, provided that Coulomb repulsion can be filtered out. Thus it is more convenient to study the dependence of the correlation function on the momentum difference and the average momentum

$$q = p_1 - p_2, \qquad K = \frac{1}{2}(p_1 + p_2).$$ (2)

The source, which produces particles, can be described with the help of a Wigner density $S(x, p)$. Its classical interpretation is that it is the probability to emit a particle with momentum p from a space–time point x. The correlation function which we express as function of q and K is then given as

$$C(q, K) - 1 \approx \frac{\left| \int d^4 x \, S(x, K) \, e^{iqx} \right|^2}{\left(\int d^4 x \, S(x, K) \right)^2}.$$ (3)

The approximation symbol stands here for two steps: (i) The on-shell approximation which replaces the time-component of K^0 ($= (p_1^0 + p_2^0)/2$) with $E_K = \sqrt{\vec{K}^2 + m^2}$, and (ii) the smoothness approximation, which assumes that the denominator can be evaluated at single value of K instead of the two momenta of the particles of the pair: $p_1 = K + q/2$ and $p_2 = K - q/2$. After some manipulations the relation can be rewritten as a simple Fourier transform:

$$C(q, K) \approx 1 + \frac{\int d^4 r \, D(r, K) \, e^{iqr}}{\left(\int d^4 x \, S(x, K) \right)^2},$$ (4)

where

$$D(r, K) = \int d^4 X \, S\left(X + \frac{r}{2}, K \right) S\left(X - \frac{r}{2}, K \right).$$ (5)

We see that the correlation function does not measure the distribution of the source itself. Instead, it is a Fourier transform of the distribution of the differences between emission points! This is important! The convolution in Equation (5) often produces a bell-shaped distribution $D(r, K)$ even for emission functions which might possess sharp edges. The Fourier transform in Equation (4) keeps this feature. This is the reason why fitting the correlation function with Gaussian does not seem such a bad idea.

Unfortunately, even measurement of the distribution $D(r, K)$ is not completely possible. Since the momenta of the particles used in the measurement must fulfil the mass-shell constraint, we have

$$q \cdot K = 0 \qquad \Rightarrow \qquad q^0 = \frac{\vec{q} \cdot \vec{K}}{K^0} = \vec{q} \cdot \vec{\beta}$$ (6)

where

$$\vec{\beta} = \frac{\vec{K}}{K^0} \approx \frac{\vec{K}}{E_K}.$$ (7)

Hence, only three components of q are independent.

In order to exploit the symmetries of the problem and simplify the interpretation of the measurement, one adopts the *out-side-long* coordinate frame. The longitudinal (or *z*) direction is parallel to the beam. The outward (or *x*) direction is identified with the direction of the transverse pair momentum K_T, so that $\vec{K} = (K_T, 0, K_l)$. The sideward (or *y*) direction is perpendicular to the above two. In this frame the Gaussian parametrisation of the correlation function reads

$$C(q, K) - 1 = \exp\left[-q_o^2 R_o^2 - q_s^2 R_s^2 - q_l^2 R_l^2 - 2q_o q_s R_{os}^2 - 2q_o q_l R_{ol}^2 - 2q_s q_l R_{sl}^2\right] . \tag{8}$$

If this parametrisation is expanded up to second order in *q* and compared with such an expansion of Equation (3), one recovers the model-independent expressions for the correlation radii [13]

$$
\begin{aligned}
R_o^2 &= \left\langle (\tilde{x} - \beta_T \tilde{t})^2 \right\rangle , & R_{os}^2 &= \langle (\tilde{x} - \beta_T \tilde{t})\tilde{y} \rangle , \\
R_s^2 &= \left\langle \tilde{y}^2 \right\rangle , & R_{ol}^2 &= \langle (\tilde{x} - \beta_T \tilde{t})(\tilde{x} - \beta_l \tilde{t}) \rangle , \\
R_l^2 &= \left\langle (\tilde{z} - \beta_l \tilde{t})^2 \right\rangle , & R_{sl}^2 &= \langle \tilde{y}(\tilde{z} - \beta_l \tilde{t}) \rangle .
\end{aligned}
\tag{9}
$$

Here, the averages are taken with the emission function

$$\langle f(x) \rangle (K) = \frac{\int d^4 x\, f(x)\, S(x, K)}{\int d^4 x\, S(x, K)} , \tag{10}$$

and the coordinates with the tilde are shifted with respect to the means

$$\tilde{x} = x - \langle x \rangle .$$

A caveat must be placed here in connection with the Expressions (9). They are well defined as long as the (co)variances of the emission function can be calculated. If the emission function, however, would be given by a Lévy stable distribution, they would not exist and the interpretation would fail. Moreover—the interpretation is even more complicated: Below we discuss how the measured correlation function results from averaging over different (effective) sources, so strictly speaking no single emission function can be assigned to the measured correlations. Nevertheless, let us consider the Expressions (9) as useful guidelines for the interpretation of measured Gaussian correlation radii.

Sometimes, poor statistics does not allow to sample the *q*-space densely enough with data so that a decent fit to the histogram can be made. In this case, a one-dimensional parametrisation of the correlation function is sometimes used, which is formulated in terms of the invariant momentum difference

$$q_{inv}^2 = q_o^2 + q_s^2 + q_l^2 - q_0^2 = |\vec{q}|^2 - (\vec{q} \cdot \vec{\beta})^2 . \tag{11}$$

In order to calculate the correlation function $C(q_{inv}, K)$ one would need to integrate both the numerator and the denominator of the three-dimensional $C(q, K)$ separately over the hypersurface in *q*-space

$$C(q_{inv}, K) = 1 + \frac{\int dq_o dq_s dq_l\, \delta(|\vec{q}|^2 - (\vec{q} \cdot \vec{\beta})^2 - q_{inv}^2)\, \left| \int d^4 x\, S(x, K) e^{iqx} \right|^2}{\int dq_o dq_s dq_l\, \delta(|\vec{q}|^2 - (\vec{q} \cdot \vec{\beta})^2 - q_{inv}^2)\, \left(\int d^4 x\, S(x, K) \right)^2} . \tag{12}$$

Note that we still assume the validity of the smoothness and the on-shell approximations.

This can be most easily interpreted in the reference frame which co-moves with the particle pair, i.e., with the velocity $\vec{\beta}$. There, all terms which contain $\vec{\beta}$ vanish, and the correlation function becomes

$$C(q_{inv}, K) = 1 + \frac{\int dq_o dq_s dq_l\, \delta(|\vec{q}|^2 - q_{inv}^2)\, \left| \int d^4 x\, S(x, K) e^{iqx} \right|^2}{\int dq_o dq_s dq_l\, \delta(|\vec{q}|^2 - q_{inv}^2)\, \left(\int d^4 x\, S(x, K) \right)^2} . \tag{13}$$

If the modification is done on the level of Gaussian parametrisation

$$C(q_{inv}, K) = 1 + \frac{1}{\mathcal{N}} \int dq_o dq_s dq_l \, \delta(|\vec{q}|^2 - q_{inv}^2) \exp\left(-q_i q_j \langle x^i x^j \rangle\right), \tag{14}$$

where

$$\mathcal{N} \equiv \int dq_o dq_s dq_l \, \delta(|\vec{q}|^2 - q_{inv}^2) \tag{15}$$

ensures that the normalization of the correlation function is unaffected by integral over the q-surface. Hence, in this frame the averaging runs over the q-surface with constant $|\vec{q}|$. The observed width of $C(q_{inv}, K)$ results from this averaging.

The value of q_{inv} can become 0 (where one would expect the maximum of the correlation function) also for non-vanishing q components (where the maximum is not expected). Therefore, a new variable has been introduced [14]

$$q_{LCMS} = \left(q_o^2 + q_s^2 + q_{l,LCMS}^2\right)^{1/2} \quad \text{where} \quad q_{l,LCMS}^2 = \frac{(p_{1z} E_2 - p_{2z} E_1)^2}{K_0^2 - K_l^2}. \tag{16}$$

Note that q_{LCMS} is invariant under longitudinal boosts. The motivation for this particular variable is that in the longitudinally co-moving frame ($K_l = 0$) it reduces just to $\sqrt{q_o^2 + q_s^2 + q_l^2}$. This variable is thus reasonable for spherically symmetric sources. We have checked that there is no dramatic qualitative difference between the results obtained with q_{inv} and those obtained with q_{LCMS} [15]. Here we shall show results obtained with q_{inv}, while results with q_{LCMS} will be shown elsewhere [15].

We have indicated in Equation (10) that the measured (co-)variances of the source depend on the pair momentum K. Why? The reason is that the particles with specified momentum only come from a part of the whole fireball, the so-called homogeneity region. If we change the momentum K, i.e., we focus on particles with different momentum, then these will be emitted from a different part of the fireball. That part also may have different size. Consequently, the sizes of the (co-)variances in Equation (9) change.

3. Averaging

We shall deal with two kinds of averaging in the discussions of the shape of the correlation function: Averaging over different momenta and averaging over many events.

Averaging over momentum comes through the binning in pair momentum K. Both histograms in q—the numerator and the denominator in Equation (1)—are constructed for $\vec{K}$ within certain interval. The bins always have finite size in the transverse component as well as in the azimuthal angle of $\vec{K}$. The latter is often even integrated over the whole 2π interval. As we pointed out, the correlation function measures the homogeneity lengths corresponding to a given $\vec{K}$. Then by taking an interval of $\vec{K}$ one makes an average over different homogeneity regions. Since the intervals of $\vec{K}$ are integrated on the level of the two histograms in Equation (1), the resulting correlation function is given as

$$C(q, K) \approx 1 + \frac{\int_{bin} dK \left| \int d^4x \, S(x, K) e^{iqx} \right|^2}{\left(\int_{bin} dK \int d^4x \, S(x, K) \right)^2}. \tag{17}$$

Averaging over events results from summing up entries to the histograms from a large number of events. Both the numerator and the denominator fluctuate from event to event, because in each event we have a fireball of different sizes and dynamical state. Averaging must therefore be carried out for the numerator and denominator separately [16,17]. We thus conclude that the correlation function will be

$$C(q, K) \approx 1 + \frac{\int dR \, \rho(R) \left| \int d^4x \, S(x, K; R) e^{iqx} \right|^2}{\int dR \, \rho(R) \left(\int d^4x \, S(x, K; R) \right)^2} \tag{18}$$

where $\rho(R)$ is the distribution of the source sizes. For brevity, we do not write out the averaging over other features of the fluctuating source explicitly; this would be implemented in the same way.

A non-Gaussian shape of the correlation function will be here fitted with the Lévy stable distribution. In one dimension is reads

$$C(q) = 1 + \lambda e^{-(qR)^\alpha} . \tag{19}$$

The three-dimensional generalisation can be formulated as [9]

$$C(q) = 1 + \lambda e^{-(q_o^2 R_o'^2 + q_s^2 R_s'^2 + q_l^2 R_l'^2)^{\alpha/2}} . \tag{20}$$

The Lévy exponent α is one of the fit parameters, together with λ and the R'''s. The value $\alpha = 2$ corresponds to Gaussian shape, meaning that a lower value ($\alpha < 2$) implies a non-Gaussian correlation function.

4. The Blast-Wave Model

For the actual calculation of various effects we will generate artificial events with the help of DRAGON Monte Carlo event generator [18,19]. It is based on the Blast-Wave (BW) model [20–24] with resonance decays included. The BW model is described by the emission function

$$S(x,K) \, d^4x = \frac{1}{(2\pi)^3} \left(\exp\left(\frac{u^\mu(x)p_\mu}{T} \right) \pm 1 \right)^{-1} \Theta(r - R(\theta)) \, \delta(\tau - \tau_{fo}) \, m_t \cosh(\eta - y)\tau \, d\tau \, d\eta \, r \, dr \, d\theta . \tag{21}$$

As spatial coordinates we use here the usual polar coordinates r and θ for the plane transverse to the beam direction, the space–time rapidity η and the longitudinal proper time τ

$$\eta = \frac{1}{2} \ln \frac{t+z}{t-z} , \qquad \tau = \sqrt{t^2 - z^2} . \tag{22}$$

Let us explain the formula representing this particular emission function.

- The factor $(2\pi)^{-3}$ stands for the elementary phase-space cell volume. Recall that $S(x,K)$ represents the distribution in phase-space. (And recall that $\hbar = c = 1$.)
- The thermal distribution—Bose-Einstein or Fermi-Dirac—is formulated with the energy in the rest frame of the fluid, $E^* = u^\mu p_\mu$, where u^μ is the (local) velocity of the fluid.
- The fireball is modelled with a sharp cutoff in the transverse direction: $\Theta(r - R(\theta))$. However, the radius R depends on the azimuthal angle in order to simulate the fireball in non-central collisions.
- Freeze out happens along a hypersurface given by constant $\tau = \tau_{fo}$.
- The fireball is manifestly boost-invariant. There is no limit set on the space–time rapidity. Nevertheless, by choosing the rapidity of particles one effectively selects just a part of the fireball (the relevant homogeneity region) which contributes to the production at that rapidity.
- The factor $m_t \cosh(\eta - y)\tau \, d\tau \, d\eta \, r \, dr \, d\theta$, where y is the rapidity of the emitted particle, comes from the Cooper-Frye [25] factor which stands for the flux of particles across the freeze-out hypersurface Σ: $p_\mu d\Sigma^\mu$.

Our model does not include any corrections to the thermal momentum distribution due to viscosity.

The transverse radius of the fireball depends on the azimuthal angle in order to implement the second-order anisotropy

$$R(\theta) = R_0 \left[1 - a_2 \cos\left(2(\theta - \theta_2) \right) \right] , \tag{23}$$

where R_0 and a_2 are model parameters, and θ_2 is the angle of the second-order event plane.

The collective expansion velocity field is parametrised with the help of η and the transverse rapidity $\eta_t(r, \theta_b)$

$$u^\mu(x) = (\cosh\eta \, \cosh\eta_t(r,\theta_b), \cos\theta_b \, \sinh\eta_t(r,\theta_b), \sin\theta_b \, \sinh\eta_t(r,\theta_b), \sinh\eta \, \cosh\eta_t(r,\theta_b)), \quad (24)$$

where the transverse rapidity depends on r and the azimuthal angle

$$\eta_t(r,\theta_b) = \rho_0 \frac{r}{R(\theta)} \left[1 + 2\rho_2 \cos(2(\theta_b - \theta_2))\right]. \quad (25)$$

The model parameters ρ_0 and ρ_2 scale the overall magnitude and the second-order oscillation of the transverse flow, respectively. We have indicated that η_t depends on θ_b, and not directly on θ. The angle θ_b gives the direction perpendicular to the surface of the fireball, and can be obtained from the relation

$$\tan\left(\theta_b - \frac{\pi}{2}\right) = \frac{dx_2}{dx_1} = \frac{\frac{dx_2}{d\theta}}{\frac{dx_1}{d\theta}} = \frac{\frac{dR(\theta)\sin(\theta)}{d\theta}}{\frac{dR(\theta)\cos(\theta)}{d\theta}}, \quad (26)$$

where the functional dependences $x_1(\theta)$, $x_2(\theta)$ refer to the transverse boundary of the fireball [26].

DRAGON also includes resonance decays. Mesonic resonances are included up to masses of 1.5 GeV, baryonic up to 2 GeV. Resonances are produced according to the same emission function as direct pions, with their pole masses. The decay vertex of a given resonance is determined according to an exponential distribution whose width is the lifetime of the resonance in question (in its rest frame): $\rho(\tau_d) \propto e^{-\Gamma_R \tau_d}$. Both two- and three-body decays are included as well as the possibility that one resonance type can decay via various channels according to their branching ratios. Cascades of decays, in which several resonances decay consecutively, are also possible within the model.

5. Results

We begin by considering the effects that the averaging over many fireballs with different shapes may have on the value of the Lévy parameter α. Indeed, in real experiments each fireball is different, with different sizes, eccentricities, and orientations of the event plane. We therefore anticipate that averaging over a distribution of source shapes, as in Equation (18), will cause α to deviate from 2. In this treatment, we limit our focus to second-order anisotropies.

With the help of DRAGON we generated sets of 50,000 events. The basic setting of the parameters includes the freeze-out temperature of 120 MeV, the average transverse radius $R = 7$ fm, freeze-out time $\tau_{fo} = 10$ fm/c, and the strength of the transverse expansion $\rho_0 = 0.8$. To keep the source simple, no resonance decays are included at this point. The correlation function is evaluated in one dimension as a function of q_{inv}.

We first study the effect of averaging over different values of a_2.

Figure 1 (left) compares the Lévy parameter α from two sets of Monte Carlo events. In the first set, all events have spatial eccentricity with $a_2 = 0.05$. In the other set, the eccentricity fluctuates with a_2 between -0.1 and 0.1. We perform the study in a narrow interval of K_T, where the shape of the correlation function changes strongly, even though it cannot be accessed experimentally (although the correlation function has been averaged over the azimuthal angle of $\vec{K}$). We see that the value of α departs from 2 considerably and reaches values between 1.27 and 1.62. The averaging makes up only a small portion of this decrease, at most at a level of 0.05.
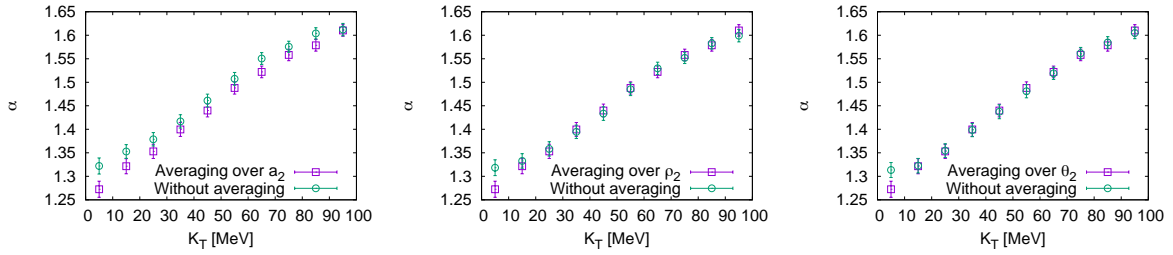
Figure 1. The Lévy parameter of the 1D fits to the correlation function in q_{inv}. Mean transverse momentum K_T in bins of 10 MeV. A green circle shows results calculated with fixed anisotropies. The purple data show results calculated for averaging over a_2 (**left**); averaging over ρ_2 (**middle**), and averaging over θ_2 (**right**). Vertical error bars show the 1σ intervals, resulting from fitting the correlation function with the ansatz of Equation (19).

Almost identical results quantitatively come from the averaging over flow anisotropy (Figure 1, middle) and the event plane orientation (Figure 1, right). In the middle panel we compare Lévy index α obtained from a set with ρ_2 fixed to 0.05 with a set with events for which ρ_2 fluctuates between -0.1 and 0.1. For the event plane averaging we see no change (except in the bin with smallest K_T) if θ_2 fluctuates in comparison to θ_2 fixed to 0. The anisotropy parameters a_2 and ρ_2 in this case fluctuate between -0.1 and 0.1.

We investigate next the influence of resonances on the obtained value of α. We use the source of direct particles with the same basic parameters as in the previous case, and we compare correlation functions obtained with and without resonance decays.

In Figure 2 we show the Lévy indices α obtained from fits to the correlation functions as a function of K_T. We know from the previous Figure already, that the one-dimensional correlation function has quite a non-Gaussian shape. Now we see that the inclusion of the resonance decays pushes down the value of α by another 0.2. The influence of resonance decays is much bigger than that of averaging over different events!
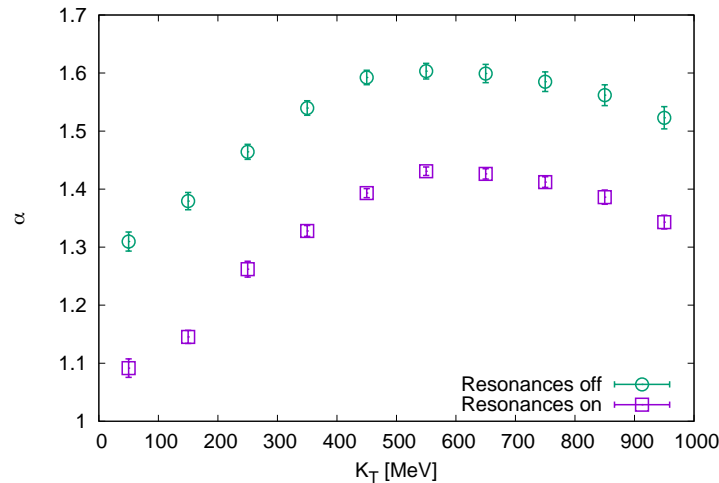

Figure 2. The Lévy parameter α of the 1D fits to the correlation function in q_{inv}. The result from the fits to the correlation function from a source without resonances (green circles) and with resonances (purple squares). Vertical error bars show the 1σ intervals.

We want to perform our analysis more differentially, however. We start by looking individually at each direction of the correlation function and fitting with the Lévy prescription of Equation (19). This is not a three-dimensional analysis, since we do not fit the correlation function in the whole q-space

and confine ourselves only to fits along the axes. The aim is to see the differences in its shape along different directions.

Indeed, we observe in Figure 3 that the differences are rather large. If resonance decays are not included, the value of α is around 2 in both transverse directions. However, in the longitudinal direction the Lévy index α is lowered to 1.8 at $K_T = 0$ and increases gradually towards 2 at $K_T = 1$ GeV. In addition, the influence of resonance decays is different for longitudinal and transverse directions. In the longitudinal direction the resonance decays cause a decrease of α by about 0.2. In the transverse directions, however, α drops as low as 1.4 once resonance decays are included.
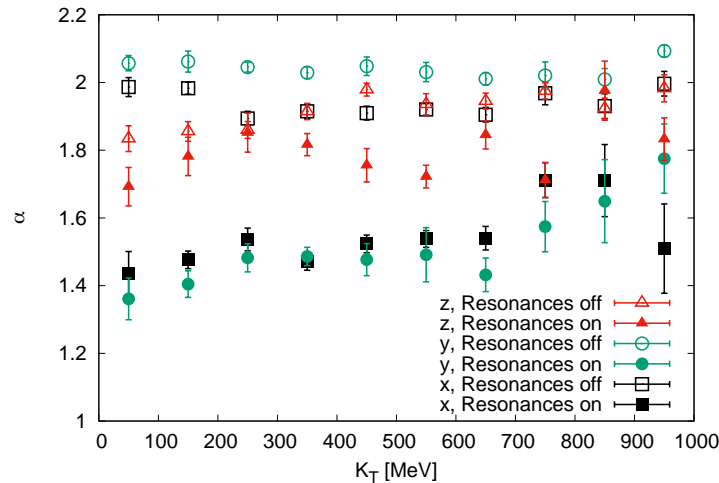
Figure 3. The Lévy parameter α from 1D fits to the correlation function in q_{inv} along the different axes, with or without resonances. Vertical error bars show the 1σ intervals, resulting from fitting the correlation function with the ansatz of Equation (19).

Note the wiggly behaviour of the data points, particularly for larger K_T. Due to the limited statistics of particle pairs, the measured values of the correlation function will tend to fluctuate. The parameter α comes from the fit to the correlation function with Equation (19). The error bars show the $\pm 1\sigma$ intervals for this particular correlation function. They underestimate the real uncertainty of the determination of α. We plan to improve the statistics and the uncertainty intervals in a forthcoming paper [15].

We would like to understand these differences and hence we checked the shape of the source which emits pions.

The profiles of the emission function are plotted in Figure 4, for pions with transverse momentum from the interval (300, 400) MeV. Note that they are produced just from a part of the whole fireball, the so-called homogeneity region. We show the distribution of the production points of pions, with pions from resonance decays included. In order to assess the effect of resonances, we also plot separately both contributions: Directly produced pions as well as those from resonance decays. The upper row shows that there is quite a difference between the longitudinal and the transverse directions. One could argue, however, that due to the on-shell constraint (6) it is not the distribution in x, that is measured, but rather the distribution in $(x - \beta_t t)$. We plot this in the lower left panel of Figure 4.

At this place we would again like to touch upon the discussion concerning the proper choice of the one-dimensional momentum difference variable (q_{inv} vs. q_{LCMS}). We recall that q_{LCMS} was introduced as a reasonable variable for spherically symmetric sources. Figure 4 shows that in this case the symmetry is not present, neither concerning the sizes, nor concerning the shape of the source in different directions.
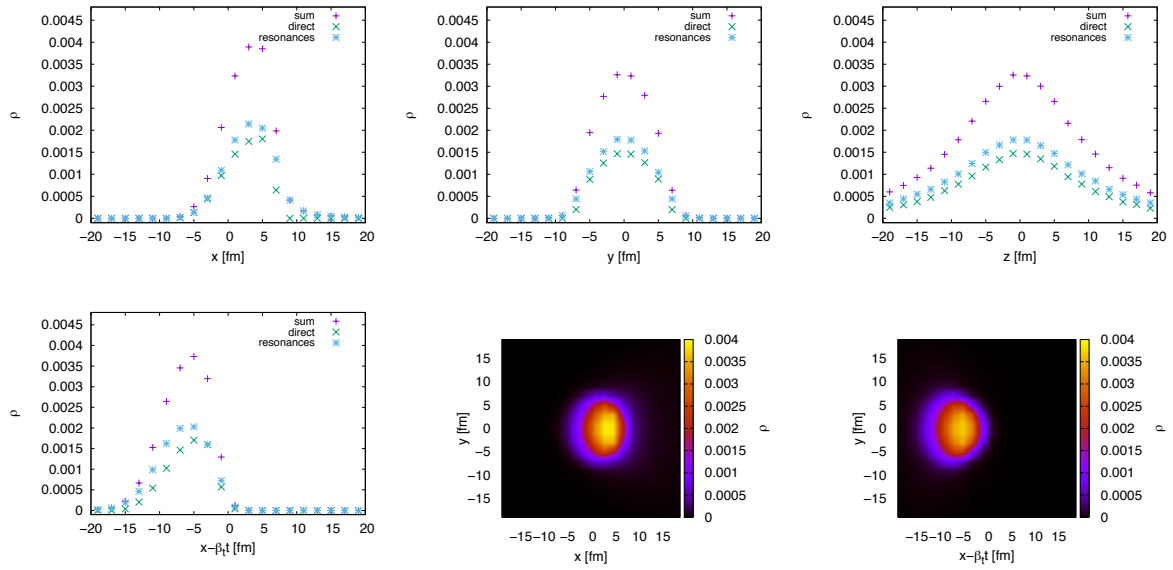
Figure 4. The spatial distribution of the emission points of pions for K_Ts. Upper row: The profiles of the emission points distribution along the x (**left**), y (**middle**), and z-axis (**right**). Lower row: The profile along the variable $(x - \beta_t t)$ (**left**), and two-dimensional distributions in the transverse plane (**middle** and **right**). A green $\times$ shows the profile of direct pions, a purple $+$ shows the profile of pions produced by resonances and a blue $*$ shows their sum. All these distributions were calculated as narrow integrals over the remaining coordinates with width 2 fm.

Finally, we extend the fitting to the whole three-dimensional correlation function from the previous simulations. The fit is performed with the three-dimensional Lévy distribution of Equation (20), so it always results in a single value of α.

This is plotted in Figure 5 as a function of K_T. We can see that the obtained α's are closer to 2 than in the case of fitting the one-dimensional correlation functions in q_{inv}, although considerable deviations from 2 are still present. Inclusion of resonance decays lowers α by about 0.1–0.3, depending on K_T.
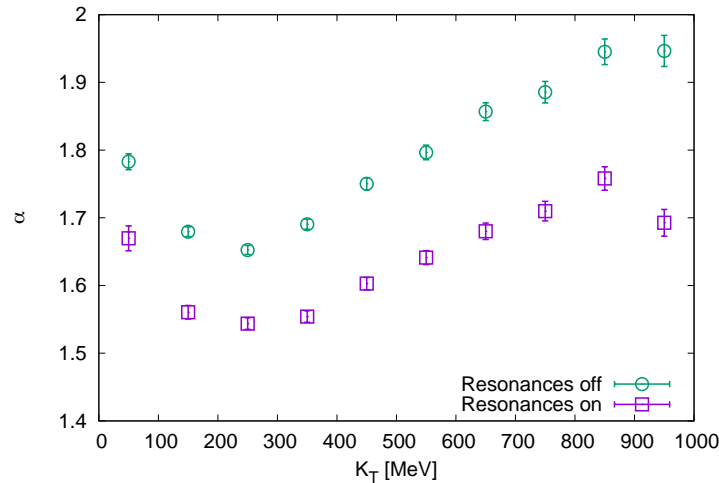

Figure 5. The Lévy parameter of the 3D fits to the correlation function according to Equation (20). Compared are simulations with and without resonances. Vertical error bars show the 1σ intervals, resulting from fitting the correlation function with the ansatz of Equation (20).

6. Conclusions

We explained in the introductory section of this paper that in addition to the generalisation of the concept of Central Limit Theorem [9], an especially important motivation for the use of Lévy stable parametrisation is the search for critical behaviour [10]. The simulations presented here show that the Lévy parameter α may clearly deviate from 2 even for "usual", non-critical sources, like those described by the blast-wave model.

Even without the presence of resonances, the shape of the correlation function looks rather non-Gaussian in the longitudinal direction. Once resonance decays are included, however, the shape deviates even further from Gaussian, especially in the two transverse directions. In this respect it appears interesting to test this with kaons, since a smaller part of them (although not negligible) comes from resonance decays.

In the three-dimensional fit, the value of α is lowered through the influence of resonance decays by about 0.1–0.3, depending on K_T.

It is very important to realise that in our simulations the biggest effect on lowering the value of α was in using only one-dimensional parametrisation of the correlation function in q_{inv}.

Author Contributions: The authors contributed to the paper in this way: conceptualization, B.T.; methodology, B.T., J.C., C.P.; software, J.C.; validation, C.P.; investigation, J.C. and B.T.; writing—original draft preparation, B.T.; writing—review and editing, J.C. and C.P.

References

1. Pratt, S. Pion Interferometry of Quark-Gluon Plasma. *Phys. Rev. D* **1986**, *33*, 1314–1327. [CrossRef]
2. Bertsch, G.; Gong, M.; Tohyama, M. Pion Interferometry in Ultrarelativistic Heavy Ion Collisions. *Phys. Rev. C* **1986**, *37*, 1896–1900. [CrossRef]
3. Makhlin, A.N.; Sinyukov, Y.M. Hydrodynamics of Hadron Matter Under Pion Interferometric Microscope. *Z. Phys. C* **1988**, *39*, 69–73. [CrossRef]
4. Pratt, S.; Csörgő, T.; Zimányi, J. Detailed predictions for two pion correlations in ultrarelativistic heavy ion collisions. *Phys. Rev. C* **1990**, *42*, 2646–2652. [CrossRef]
5. Chapman, S.; Scotto, P.; Heinz, U. A new cross term in the two particle HBT correlation function. *Phys. Rev. Lett.* **1995**, *74*, 4400–4403. [CrossRef] [PubMed]
6. Kincses, D. Lévy Analysis of HBT Correlation Functions in s N N = 62 GeV and 39 GeV Au + Au Collisions at PHENIX. *Universe* **2018**, *4*, 11. [CrossRef]
7. Kurgyis, B. Three-dimensional Lévy HBT Results from PHENIX. *Acta Phys. Pol. B Proc. Suppl.*, **2019**, *12*, 477. [CrossRef]
8. Pórfy, B. Levy HBT results at NA61/SHINE. *Universe*, under review.
9. Csörgő, T.; Hegyi, S.; Zajc, W.A. Bose-Einstein correlations for Lévy stable source distributions. *Eur. Phys. J. C* **2004**, *36*, 67–78. [CrossRef]
10. Csörgő, T. Correlation Probes of a QCD Critical Point. *PoS HIGH-PTLHC* **2008**, *8*, 027.
11. Bowler, M.G. Coulomb corrections to Bose-Einstein correlations have been greatly exaggerated. *Phys. Lett. B* **1991**, *270*, 69–74. [CrossRef]
12. Sinyukov, Y.; Lednický, R.; Akkelin, S.V.; Pluta, J.; Erazmus, B. Coulomb corrections for interferometry analysis of expanding hadron systems. *Phys. Lett. B* **1998**, *432*, 248–257. [CrossRef]
13. Chapman, S.; Scotto, P.; Heinz, U. Model independent features of the two particle correlation function. *Acta Phys. Hung. A* **1995**, *1*, 1–31.

14. Adare, A.; Aidala, C.; Ajitanand, N.N.; Akiba, Y.; Akimoto, R.; Alexander, J.; Alfred, M.; Al-Ta'ani, H.; Angerami, A.; Aoki, K.; et al. [PHENIX Collaboration]. Lévy-stable two-pion Bose-Einstein correlations in $\sqrt{s_{NN}} = 200$ GeV Au+Au collisions. *Phys. Rev. C* **2018**, *97*, 064911. [CrossRef]

15. Cimerman, J.; Plumberg, C.; Tomášik, B. Unpublished work, 2019, in preparation.

16. Plumberg, C.J.; Shen, C.; Heinz, U.W. Hanbury-Brown–Twiss interferometry relative to the triangular flow plane in heavy-ion collisions *Phys. Rev. C* **2013**, *88*, 044914; Erratum: *Phys. Rev. C* **2013**, *88*, 069901.

17. Plumberg, C.; Heinz, U. Probing the properties of event-by-event distributions in Hanbury-Brown–Twiss radii. *Phys. Rev. C* **2015**, *92*, 044906; Addendum: *Phys. Rev. C* **2015**, *92*, 049901. [CrossRef]

18. Tomášik, B. DRAGON: Monte Carlo generator of particle production from a fragmented fireball in ultrarelativistic nuclear collisions. *Comput. Phys. Commun.* **2009**, *180*, 1642–1653. [CrossRef]

19. Tomášik, B. DRoplet and hAdron generator for nuclear collisions: An update. *Comput. Phys. Commun.* **2016**, *207*, 545–546. [CrossRef]

20. Siemens, P.J.; Rasmussen, J.O. Evidence for a blast wave from compress nuclear matter. *Phys. Rev. Lett.* **1979**, *42*, 880–887. [CrossRef]

21. Schnedermann, E.; Sollfrank, J.; Heinz, U. Thermal phenomenology of hadrons from 200-A/GeV S+S collisions. *Phys. Rev. C* **1993**, *48*, 2462–2475. [CrossRef]

22. Csörgő, T.; Lörstad, B. Bose-Einstein correlations for three-dimensionally expanding, cylindrically symmetric, finite systems. *Phys. Rev. C* **1996**, *54*, 1390–1403. [CrossRef]

23. Tomášik, B.; Wiedemann, U.A.; Heinz, U. Reconstructing the freezeout state in Pb + Pb collisions at 158 GeV/c. *Acta Phys. Hung. A* **2003**, *17*, 105–143. [CrossRef]

24. Retiere, F.; Lisa, M.A. Observable implications of geometrical and dynamical aspects of freeze out in heavy ion collisions. *Phys. Rev. C* **2004**, *70*, 044907. [CrossRef]

25. Cooper, F.; Frye, G. Comment on the Single Particle Distribution in the Hydrodynamic and Statistical Thermodynamic Models of Multiparticle Production. *Phys. Rev. D* **1974**, *10*, 186. [CrossRef]

26. Cimerman, J.; Tomášik, B.; Csanád, M.; Lökös, S. Higher-order anisotropies in the Blast-Wave Model - disentangling flow and density field anisotropies. *Eur. Phys. J. A* **2017**, *53*, 161. [CrossRef]